AIMS Environmental Science

AIMS Environmental Science, 11(6): 883–899.
DOI: 10.3934/environsci.2024044
Received: 18 July 2024
Revised: 30 August 2024
Accepted: 09 September 2024
Published: 14 October 2024

https://www.aimspress.com/journal/environmental

Research article

Synthesis and development of $Fe_3O_4/SiO_2/CaCO_3$ nanocomposite adsorbents for ammonia adsorption in the shrimp pond waste

Lukluatus Syavika, Anugrah Ricky Wijaya* and Alif Alfarisyi Syah

Department of Chemistry, Faculty of Mathematic and Sciences, Universitas Negeri Malang (UM) or State University of Malang, Jl. Semarang 5 Malang 65145, Indonesia

* **Correspondence:** Email: anugrah.ricky.fmipa@um.ac.id.

Abstract: We developed a $Fe_3O_4/SiO_2/CaCO_3$ magnetic nanocomposite adsorbent, with SiO_2 synthesized from sea sand and $CaCO_3$ derived from coral skeletons. The $Fe_3O_4/SiO_2/CaCO_3$ nanocomposite was characterized and employed as an adsorbent to reduce ammonia levels in shrimp pond wastewater where ammonia concentrations ranged from 11.9 to 38.8 mg/L. We further explored the effects of various parameters on the removal efficiency, adsorption capacity, thermodynamics, isoterm, and kinetics of the adsorption process. Specifically, we examined the influence of pH (3–8), adsorbent mass (0.025–0.25 g), temperature (27–60 °C), and contact time (10–120 min). Ammonia concentrations in the filtrate were measured using the Nessler method. The synthesis of $CaCO_3$ from coral skeleton, SiO_2 from sand, and $Fe_3O_4/SiO_2/CaCO_3$ adsorbent was successfully achieved, as confirmed by XRF, FTIR, and XRD characterizations. The adsorption process adhered to the second-order kinetics model, exhibited spontaneous behavior with a negative ΔG value, and followed the Langmuir isotherm model (R^2 = 0.9267). The results indicated an optimal adsorbent mass of 0.025 g, achieving 89.3% adsorption at 60 minutes of contact time, a temperature of 27 °C, and an optimal pH of 5. When applied to shrimp pond wastewater, the $Fe_3O_4/SiO_2/CaCO_3$ adsorbent demonstrated an adsorption efficiency ranging from 52.1% to 86.8% and an adsorption capacity between 6.2 and 30.9 mg/g.

Keywords: ammonia; adsorbent; adsorption; Nessler; sea sand; coral skeleton

1. Introduction

The Gulf of Prigi is considered a natural resource, situated far from major cities, thus remaining

uncontaminated by pollutants and heavy metals [1,2]. Prigi serves a national port, directly connected to surrounding villages, and is a popular beach destination with significant tourist activity [3]. The local community frequently utilizes the Prigi coastline for fishing, tourism, maritime transportation, and settlement [4]. However, the increasing construction of shrimp ponds around the gulf poses potential environmental risks if waste from these ponds is discharged into the sea without proper treatment. Shrimp wastewater must be treated to reduce ammonia levels before being released into the environment. Ammonia-contaminated seawater can be hazardous to all life forms, particularly marine and human species. Excessive ammonia also reduces the oxygen levels in the environment.

One effective and straightforward method to reduce excess ammonia in shrimp wastewater is adsorption. Sand and coral skeletons from the Gulf of Prigi, rich in SiO_2 and $CaCO_3$, can be used as adsorbents. Sand with a silica content of 60–70% is essential for producing pure silica, while coral with over 90% calcium content is ideal for synthesizing calcium carbonate. Here, we combined the Fe_3O_4 with SiO_2 and $CaCO_3$ to create a $Fe_3O_4/SiO_2/CaCO_3$ nanocomposite, which leverages the magnetic properties of nano-magnetite and the homogeneity of the composite to effectively adsorb in shrimp wastewater.

Co-precipitation is a simple, energy-efficient technique for producing nano magnetite and highly pure, homogenous, small-sized nanomaterials [5]. The advantage of using magnetic adsorbents is their ease of separation, as they do not require filtration or centrifugation, unlike other adsorbents [6]. We developed an adsorption method using synthesized $Fe_3O_4/SiO_2/CaCO_3$ nanocomposites to reduce ammonia levels in shrimp pond wastewater prior to disposal. The character and influence of mass, contact time, temperature, and pH on the adsorption process were also examined. Following characterization, we measured the ammonia concentrations before and after treatment with adsorbents using the Nessler method. This method, which detects ammonia by reacting with K_2HgI_4 (Nessler's reagent) to produce a yellow to brownish-yellow colloidal dispersion [7], was applied to assess ammonia concentration and adsorption efficiency. The synthesis of the $Fe_3O_4/SiO_2/CaCO_3$ nano adsorbent involved three steps: Extracting SiO_2 from sea sand, obtaining $CaCO_3$ from coral skeleton, and synthesizing Fe_3O_4, which was then applied to remove ammonia from shrimp waste water.

2. Materials and methods

2.1. Materials

Nessler reagent, 50% potassium sodium tartrate solution, $FeCl_3 \cdot 6H_2O$, $FeSO_4 \cdot 7H_2O$, NH_4OH, HCl, Na_2CO_3, NH_4Cl, and HNO_3 were obtained from Duta Jaya Laboratory Supply (Indonesia). The reagents were of analytical grade and were used without further purification.

2.2. Methods

2.2.1. Extraction of SiO_2 from sea sand

The sea sand was dried and reacted with a mixture of concentrated HCl and HNO_3 by reflux, then calcined at a temperature of 800 °C. The calcination results were digested with concentrated HCl until it is formed, and then the precipitate was neutralized and calcined at a temperature of 600 °C.

2.2.2. Extraction of $CaCO_3$ from coral skeleton

The Coral skeleton was dried in an oven at 60 °C, then ground using a mortar and pestle. The ground sample was sieved with a 200-mesh sieve, and placed in a furnace at 600 °C for 2 hours. The sample was then treated with 100 mL of 3 mol/L HCl solution until it became homogeneous. After precipitation, the sample was filtered, and the supernatant was treated with 150 mL of 0.6 mol/L Na_2CO_3 solution.

2.2.3. Synthesis of Fe_3O_4

$FeCl_3 \cdot 6H_2O$ and $FeSO_4 \cdot 7H_2O$ were dissolved in 150 mL of distilled water. The resulting $FeCl_3$ and $FeSO_4$ solutions were combined and heated to 90 °C using a magnetic stirrer. Once the solution reached 90 °C, 10 mL of 25% NH_4OH solution was added, and the mixture was stirred and heated for 30 mins. The solution was then allowed to cool, before being filtered to obtain a black precipitate, which was thoroughly rinsed and neutralized with distilled water.

2.2.4. Synthesis of $Fe_3O_4/SiO_2/CaCO_3$ nanocomposite

A total of 0.5 g of PEG 4000 was melted at 60 °C and combined with 0.7 g of solid Fe_3O_4, stirring until thoroughly mixed. Then, 0.7 g of SiO_2 and $CaCO_3$ were added, and the mixture was stirred until it was homogeneous. The resulting nanocomposite was placed in an oven at 40 °C.

2.2.5. Characterization of Fe_3O_4 and $Fe_3O_4/SiO_2/CaCO_3$ composites.

The initial characterization of the Fe_3O_4 and $Fe_3O_4/SiO_2/CaCO_3$ nanoparticles was performed using a FT-IR (Shimadzu IR Prestige 21) to identify the functional groups of the compounds. XRD (PANalytical X'Pert Pro) was subsequently used to assess the crystallinity of the samples. Vibrating-Sample Magnetometry (VSM, DXV-100~550 Series) was employed to determine the magnetic moment.

2.2.6. Application of adsorbents to standard ammonium solution

Twenty-five mL of standard NH_4Cl solution (4 mg/L) was treated with varying masses of adsorbent (0.025–0.25 g) and shaken at 150 rpm, under varying contact time (10–120 min), temperatures (27–60 °C), and pH levels (3–10). The filtrate was then analyzed using the Nessler method.

2.2.7. Application of adsorbents to shrimp pond wastewater

Twenty-five mL of shrimp pond wastewater was treated with the optimum mass of adsorbent and shaken at 150 rpm for the optimal contact time. The filtrate was subsequently analyzed using the Nessler method.

2.2.8. Ammonia test using the Nessler method

Ten mL of the sample filtrate was reacted with 0.5 mL of K-Na tartrate solution and 1 mL of Nessler's reagent at a wavelength of 420 nm. Samples containing ammonia developed a yellow to

brownish-yellow coloration.

3. Results and discussion

3.1. Synthesis of SiO_2 from sea sand

The sea sand was analyzed using XRF to determine the composition of oxide compounds, focusing on the Si content in the material before and after the extraction process (Table 1).

Table 1. Mineral composition of sea sand before and after extraction, and coral skeleton.

Compound/Element	Content (%At or Wt)		
	Sea sand before extraction	Sea sand after extraction	Coral Skeleton
SiO_2	16.2	89.5	-
CaO	42.2	4.55	-
TiO_2	4.6	1.86	-
Fe_2O_3	32.1	3.09	-
SrO	1.6	0.16	-
MnO	0.3	0.09	-
Ca	-	-	90.62
Fe	-	-	1.7
Si	-	-	1.3

The silica extracted from the sand was analyzed using XRF and FT-IR to assess its purity. The XRF results indicate that the produced silica contains 89.5% SiO_2 (Table 1). This represents a significant increase in SiO_2 levels, from 16.2% before extraction to 89.5% afterward, demonstrating the effectiveness of the extraction process in purifying silica from sea sand. The use of a mixture of HCl and HNO_3 was successful in removing metal impurities, such as Fe and Ca, which are present in the sand as carbonate compounds. The extraction method, which employed the destruction technique, proved to be quite effective in eliminating these impurities, resulting in a final product with a significantly higher silica content. This purified silica is better suited for use as an adsorbent, particularly for applications involving ammonia.

Figure 1 illustrates several absorption peaks at wave numbers 804.31, 1159.5, and 1045.41 cm^{-1}, corresponding to the bending vibrations, asymmetric stretching vibrations, and stretching vibrations of the Si-O group within the siloxane group (Si-O-Si), respectively. Additionally, the absorption observed at 1612.49 cm^{-1} is attributed to the -OH group associated with the Si-OH bond. The absorption at 3365.78 cm^{-1} corresponds to the stretching vibration of the extended -OH functional group, indicating the presence of the silanol (Si-OH) functional group [8].

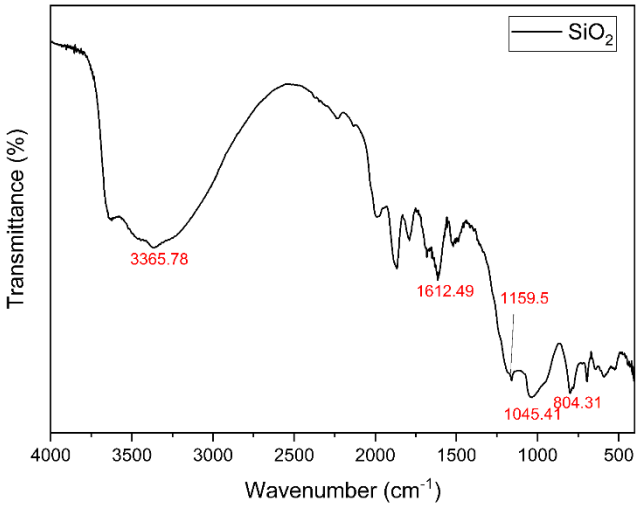

Figure 1. Spectrum of extracted SiO_2.

Figure 2 presents the XRD analysis of the synthesized SiO_2. The XRD characterization reveals sharp peaks, which is indicative of the presence of nanocomposites in the crystal phase. Distinct peaks are observed with 2 theta values of 20.7; 26.36; 36.44; 42.36; 50.26, corresponding to the (101), (111), (200), (211), and (212) planes of SiO_2, respectively, which agrees with the findings of Jiang et al. [9]. The sharp and well-defined peaks in the XRD pattern confirm the crystalline nature of the synthesized silica. Crystalline silica is characterized by regular porosity with well-defined pore sizes and shapes, making it suitable for tailoring pore size to meet the specific requirements of adsorption applications.

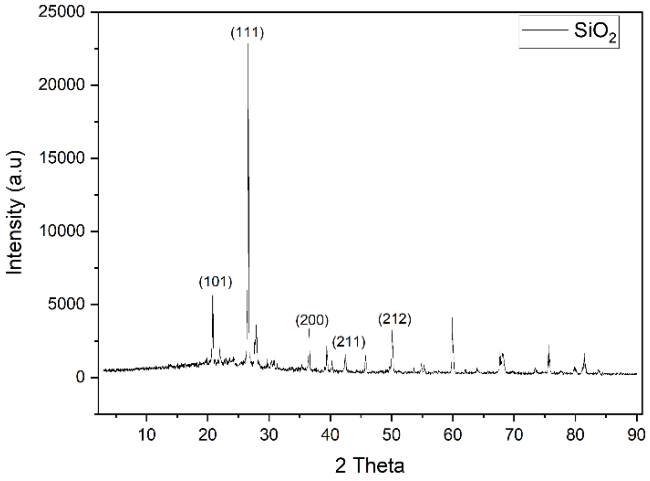

Figure 2. XRD spectra of SiO_2.

3.2. Synthesis of $CaCO_3$ from coral skeleton

Coral is rich in calcium, as detailed in Table 1 XRF results show that coral contains more than 90% calcium. The calcium was extracted from the coral to produce calcium carbonate ($CaCO_3$), which was subsequently analyzed using FT-IR, with the results shown in Figure 3.

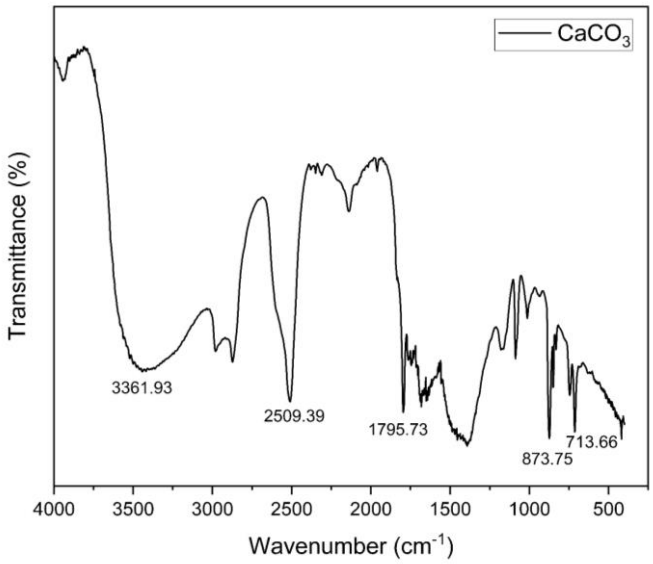

Figure 3. FT-IR spectrum of extracted $CaCO_3$.

The extraction of calcium carbonate begins with drying the coral, followed by grinding it into a fine powder and sifting it through a 200-mesh sieve. Next, 10 g of the coral powder was heated in a furnace at 600 °C for 2 hours to remove water and inorganic impurities. After this heating process, a 3 mol/L HCl solution was added to dissolve the calcium, forming $CaCl_2$ as described in Reaction Eq 1. The resulting precipitate was filtered out, and a 0.6 mol/L Na_2CO_3 solution was then added to the filtrate, yielding white $CaCO_3$ according to Reaction Eq 2, as follows:

$$\mathrm{CaCO_3(Coral\ \ Skeleton)}(s) + 2\mathrm{HCl}(aq) \rightarrow \mathrm{CaCl_2}(aq) + \mathrm{CO_2}(g) + \mathrm{H_2O}(l) \quad (1)$$

$$\mathrm{CaCl_2}(aq) + \mathrm{Na_2CO_3}(aq) \rightarrow \mathrm{CaCO_3}(s) + 2\mathrm{NaCl}(aq) \quad (2)$$

The $CaCO_3$ synthesized from coral was analyzed using FT-IR, with the resulting spectrum presented in Figure 3 The adsorption bands at wavenumbers 713.66, 873.75, 1795.73 cm^{-1} correspond to the Ca-C bond, the carbonate ion (CO_3^{2-}), and the carbonyl group (C=O) in $CaCO_3$ [10], respectively.

Figure 4 presents the XRD pattern of the synthesized $CaCO_3$. The XRD analysis reveals sharp peaks at 2θ values of 25; 27.04; 29.42; 32.88; 36.1, corresponding to (100), (101), (104), (102), and (110) planes of $CaCO_3$, respectively, as reported by other researchers [11].

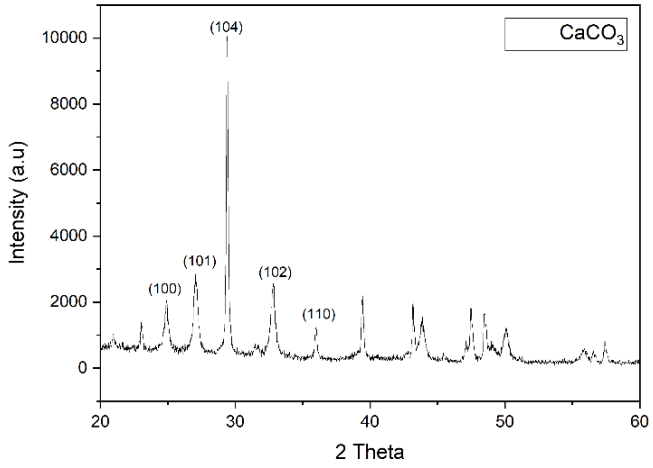

Figure 4. Spectra of synthesized $CaCO_3$.

3.3. Synthesis Fe_3O_4

Fe_3O_4 was synthesized using a mixture of $FeCl_3$ and $FeSO_4$. Upon the addition of NH_4OH, a black solution formed, indicating the formation of Fe_3O_4. The reaction resulted in a coal-black precipitate composed of Fe_3O_4 particles. The chemical reaction for the formation of Fe_3O_4 through the combination of $FeCl_3$ and $FeSO_4$ is represented in Eq 3, as follows:

$$2FeCl_3(aq) + FeSO_4(aq) + 8NH_4OH(aq) \rightarrow Fe_3O_4(s) + (NH_4)_2SO_4(aq) + 6NH_4Cl(aq) + 4H_2O(aq) \quad (3)$$

As illustrated in Figure 5, the XRD characterization of the synthesized Fe_3O_4 reveals sharp peaks, indicating the presence of nanocomposites in the crystal phase. The XRD pattern displays distinct diffraction peaks corresponding to pure Fe_3O_4, which have been compared with the Crystallography Open Database (ID: 1011032). Specific fractional peaks are observed at 2θ values of 18.25, 30.18, 35.55, 43.20, 53.57, and 62.78, corresponding to the (111), (220), (311), (400), (422), (511), and (440) planes of Fe_3O_4, respectively, as reported by Nanlohy et al. [11].

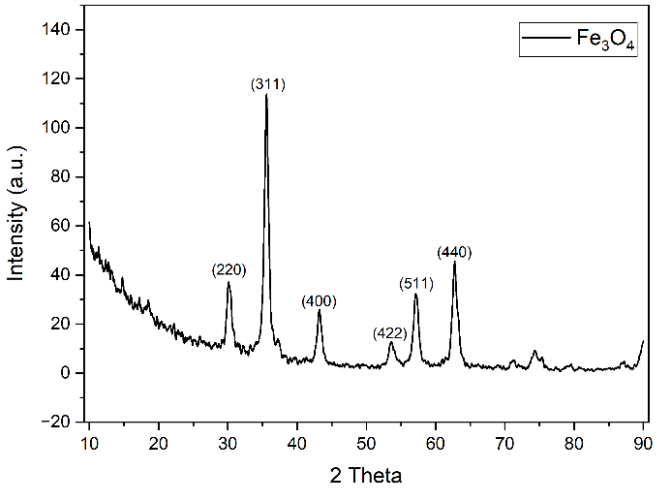

Figure 5. XRD analysis of Fe_3O_4.

3.4. Synthesis $Fe_3O_4/SiO_2/CaCO_3$

The synthesis of the $Fe_3O_4/SiO_2/CaCO_3$ adsorbent was performed by mixing each compound with PEG as an adhesive agent. The resulting adsorbent was characterized using XRD analysis, with the results presented in Figure 6.

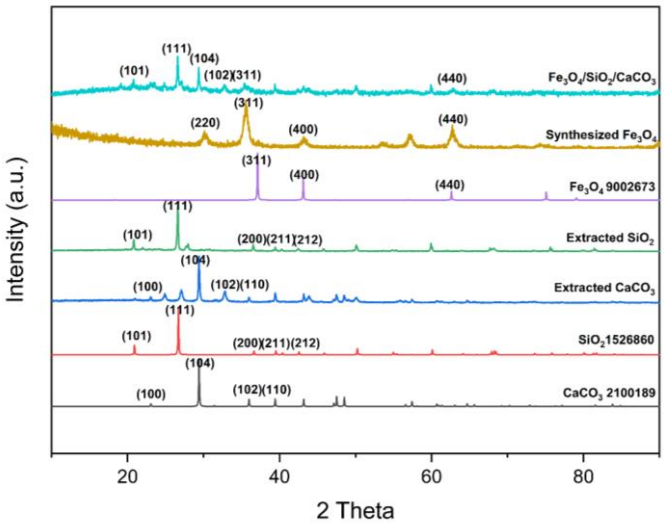

Figure 6. XRD analysis of $Fe_3O_4/SiO_2/CaCO_3$.

XRD analysis reveals multiple sets of diffraction peaks corresponding to the different phases of the $Fe_3O_4/SiO_2/CaCO_3$ composite. These peaks appear at specific angular positions that reflect the crystallinity and crystal structure of each component. The width of the diffraction peaks provides insights into crystal size and structural imperfections; broader peaks may suggest larger crystal sizes or defects within the crystallites.

The composite was further characterized using SEM-EDX. SEM images of the adsorbent, shown in Figure 7, reveal particle sizes ranging from 70 to 100 nm, with an average diameter of 78.95 nm (as depicted in Figure 8). EDX analysis confirms the presence of Fe, Si, Ca, C, and O, with weight percentages of 6.9%, 0.9%, 15.6%, 39.4%, and 37%, respectively.

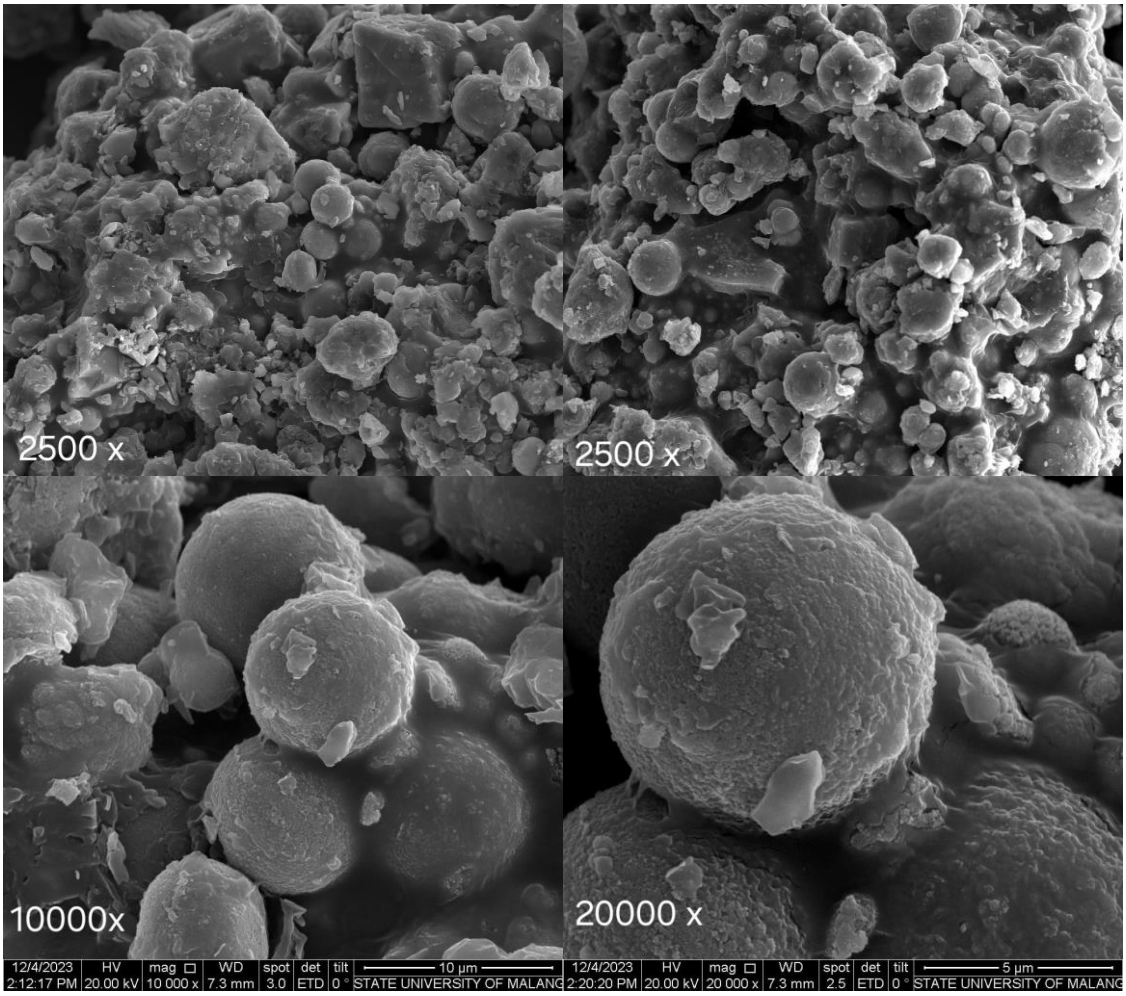

Figure 7. SEM images of $Fe_3O_4/SiO_2/CaCO_3$

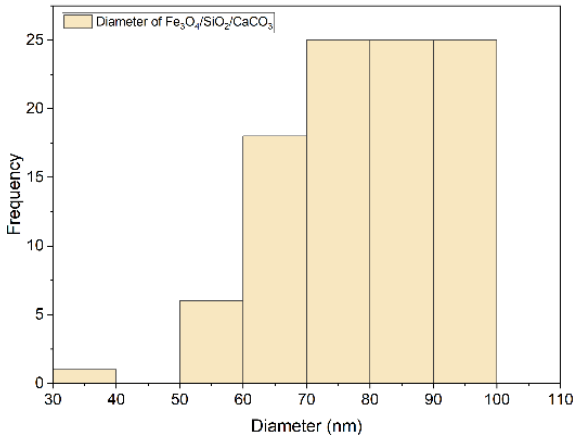

Figure 8. Diameter histogram of $Fe_3O_4/SiO_2/CaCO_3$.

The VSM characterization is depicted in the hysteresis curve in Figure 9. As shown in Table 2, the saturation magnetization (Ms), remanent magnetization (Mr), and coercivity field (Hc) of $Fe_3O_4/SiO_2/CaCO_3$ are lower than those of Fe_3O_4 alone due to the compositing effect of SiO_2 and $CaCO_3$, which reduces the magnetic properties. However, the magnetic properties of $Fe_3O_4/SiO_2/CaCO_3$ remain sufficiently high and were successfully tested using an external magnet. Magnetic materials with an Ms value between 10–20 emu/g exhibit a significant magnetic response, making them suitable as adsorbents.

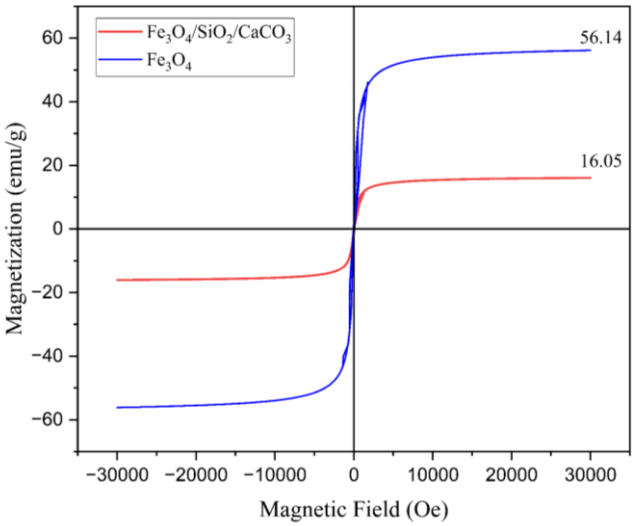

Figure 9. VSM Analysis of $Fe_3O_4/SiO_2/CaCO_3$ and Fe_3O_4.

Table 2. Magnetic properties of Fe_3O_4 and $Fe_3O_4/SiO_2/CaCO_3$.

	Hc (Tesla)	Ms (emu/g)	Mr (emu/g)
Fe_3O_4	0.06	56.14	2.19
$Fe_3O_4/SiO_2/CaCO_3$	0.087	16.05	5.29

3.5. Application of adsorbent to standard ammonia solution

The effect of adsorbent mass on the adsorption of a 4 mg/L ammonia standard solution is presented in Table 3. The optimal adsorbent mass was determined to achieve maximum ammonia adsorption capacity. A smaller adsorbent mass can provide easier access for ammonia molecules to interact with the available adsorption sites on the surface, thereby increasing adsorption efficiency. This occurs because the target molecules can more readily reach the adsorption sites. The decrease in adsorption percentage with increasing adsorbent mass can be attributed to several factors. First, the number of available adsorption sites on the adsorbent may be limited. Once these sites are occupied, adding more adsorbent does not increase the adsorption percentage, as no additional sites are available. Additionally, increasing the mass of the adsorbent may lead to interactions between the adsorbent particles, potentially reducing their individual affinity or adsorption capacity. This interaction can cause a decrease in the adsorption percentage even as the adsorbent mass increases. Furthermore, the saturation point may be reached, where adding more adsorbent mass no longer enhances adsorption because all available sites are fully occupied. An adsorbent mass of 0.025 g achieved the highest

ammonia adsorption efficiency, with a maximum of 89.3%.

Table 3. Data on % adsorption for variations in mass, contact time, temperature, and pH in ammonia standard solution.

Mass (g)	% adsorption	Contact time (minutes)	% adsorption	Temperature (°C)	% adsorption	pH	% adsorption
0.025	89.3	10	80.3	27	89.3	3	85.9
0.05	87.7	20	83.9	30	69.7	5	89.3
0.1	67.8	30	85.1	40	79.6	6	83.8
0.25	81.5	40	87.3	50	50.0	7	86.1
		50	88.9	60	76.1	8	80.8
		60	89.3			9	85.2
		120	75.8			10	85.3

The effect of contact time on the adsorption of the 4 mg/L standard solution is listed in Table 3. As the contact time increases, the amount of ammonia adsorbed decreases, likely due to the re-dissolution of ammonia back into the solution during prolonged contact. An adsorbent with a contact time of 60 minutes achieved an ammonia adsorption efficiency of 89.3%. The effect of temperature on the adsorption of the 4 mg/L standard solution is also presented in Table 3. At higher temperatures, the ammonia could not be detected, likely due to its evaporation. The optimal temperature for ammonia adsorption was 27 °C (room temperature), with a maximum adsorption efficiency of 89.3%. Activation energy, pore structure stability, and reaction kinetics may contribute to the optimal adsorption conditions at room temperature. This is supported by the negative ΔG value shown in Table 3, indicating that the adsorption process is spontaneous and does not require additional conditions like high temperature or pressure.

The effect of pH on the adsorption of the 4 mg/L standard solution is also shown in Table 3. The optimal pH for ammonia adsorption was found to be pH 5, with an efficiency of 89.3%. Deviations from this pH, either higher or lower, result in less effective adsorption. pH variations can alter the chemical equilibrium in the adsorption system, affecting the chemical species present in the solution and thereby impacting the adsorbent's specific adsorption capacity.

3.6. Adsorption kinetics

The kinetics of ammonia adsorption were studied by analyzing the amount adsorbed over varying contact times, ranging from 10 to 60 minutes. The obtained data were analyzed using two kinetic models: The pseudo-first-order and pseudo-second-order adsorption kinetics. The linear equations representing these two models can be expressed as follows [11]:

$$ln\ ln\ (q_e - q_t) = lnq_e - k_1 t \tag{4}$$

$$\frac{t}{q_t} = \frac{1}{k_2 q_e^2} + (\frac{1}{q_e})t \tag{5}$$

In this formula, q_e and q_t represent amount of ammonia adsorbed at equilibrium and a specific time, respectively (mg/g). The constant k_1 is the rate constant for the pseudo-first-order model (min^{-1}), while k_2 is the rate constant for the pseudo-second-order model (g/mg.m). The values of k_1 and k_2 are

determined from the slope of the respective linear plots shown in Figure 10. For the pseudo-first-order model, the graph is plotted as $\ln(q_e-q_t)$ versus contact time (minutes), while for the pseudo-second-order model, the graph is plotted as t/q_t versus contact time (minutes). The adsorption kinetic parameters derived from these models are summarized in Table 4.

Based on the calculated adsorption kinetic parameters in Table 4, the adsorption process follows the pseudo-second-order kinetic model, as indicated by the coefficient of determination (R^2) value being closest to 1. The rate constant k is a crucial parameter in adsorption kinetics, indicating the speed at which the adsorption process occurs. A smaller k value corresponds to a faster adsorption process. Additionally, the uniformity of the adsorbent material's particle size significantly influences the kinetics of adsorption, consistent with the pseudo-second-order model. As shown in Figure 8, the adsorbent particles range in size from 70–100 nm, indicating a high degree of size uniformity.

Table 4. Calculated kinetics, thermodynamics, and adsorption isotherm data for ammonia by $Fe_3O_4/SiO_2/CaCO_3$ adsorbents.

Parameter						
Adsorption Kinetic						
Pseudo first order	q_{exp} (mg/g)		$q_{e,cal}$ (mg/g)		k_1 (min^{-1})	R^2
	3.79		1.154		–0.079	0.872
Pseudo second order	$q_{e,cal}$ (mg/g)		k_2 (g/mg•m)		R^2	
	3.89		0.142		0.999	
Adsorption Thermodynamic						
	ΔG (kJ/mol)				ΔH (kJ/mol)	ΔS (kJ/mol.K)
	300 K	303 K	313 K	323K	–54.05	–0.17
	–4.14	–3,64	–1.98	–0.32		
Adsorption Isotherm						
Langmuir	q_{max}		b		R^2	K_L
	0.954		0.2		0.927	5.238
Freundlich	K_F		1/n		R^2	
	0.824		0.612		0.899	

3.7. Adsorption thermodynamics

Adsorption thermodynamics were studied to understand the effect of temperature on the adsorption process, specifically whether the process is endothermic or exothermic, and whether it occurs spontaneously or non-spontaneously. Temperature variations of 27, 30, 40, and 50 °C were applied. As shown in Table 4, the negative ΔH value indicates that ammonia adsorption by the $Fe_3O_4/SiO_2/CaCO_3$ adsorbent is an exothermic process, involving weak attraction forces between the adsorbent and adsorbate. Moreover, the negative ΔG value signifies that the adsorption process is spontaneous and does not require external energy. A negative ΔS value suggests a decrease in the degree of disorder at the liquid-solid interface during the ammonia adsorption process, leading to a more ordered arrangement of ammonia molecules on the adsorbent surface.

3.8. Adsorption isotherm

Adsorption isotherms describe the relationship between the concentration of a substance adsorbed on the surface of an adsorbent material and the concentration of that substance in the surrounding liquid or gas phase. They provide valuable information about the maximum adsorption capacity of an adsorbent for specific substances. Determining the adsorption isotherm helps in understanding the interactions between adsorbent molecules and the surface, as well as the surface properties of the material, based on molecular interactions at the microscopic level.

Adsorption follows the Langmuir isotherm model, as evidenced by a coefficient of determination (R^2) value closest to 1. This indicates that the adsorption process occurs on a uniform surface with identical adsorption sites, meaning there is no change in the affinity of the adsorbent across different sites, and each site can capture only one molecule. In other words, the adsorption is monolayer, and multilayer adsorption does not occur [12].

As shown in Figure 10 and Table 4, the Langmuir isotherm model for the ammonia adsorption process by the $Fe_3O_4/SiO_2/CaCO_3$ adsorbent has an R^2 value of 0.927, which is closer to 1 than the R^2 value for the Freundlich isotherm. This suggests that the adsorption process is chemical and occurs in a single layer of the adsorbent at a constant temperature [13]. The q_{max} value, representing the maximum adsorption capacity of ammonia by the adsorbent, is 0.954 mg/g. This maximum capacity can be achieved by optimizing the parameters affecting adsorption capacity. The lower value of b compared to K_F indicates that adsorption is dependent on temperature and the enthalpy of adsorption. The Freundlich isotherm model shows a 1/n value, representing adsorption intensity or surface heterogeneity of 0.612, which is less than 1, indicating favorable adsorption [14]. The K_F value, a relative indicator of maximum adsorption capacity related to the binding energy of the adsorbent, shows that the maximum adsorption capacity of ammonia by the $Fe_3O_4/SiO_2/CaCO_3$ adsorbent is 0.824 mg/g.

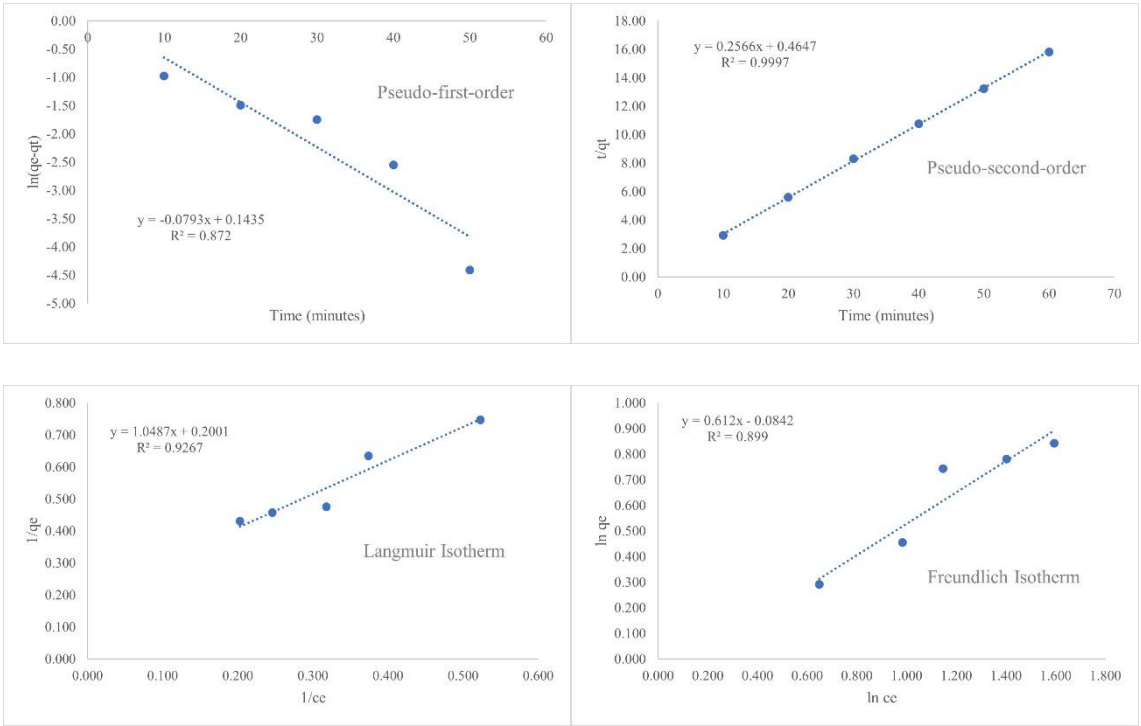

Figure 10. Adsorption kinetic and isotherms of $Fe_3O_4/SiO_2/CaCO_3$.

3.9. Shrimp pond wastewater samples

The optimized adsorption method was applied to shrimp pond wastewater samples. The ammonia content in these samples ranged from 11.9 to 38.8 mg/L, exceeding the specified quality standard threshold. The maximum allowable ammonia concentration in shrimp pond wastewater is 0.3 mg/L. Reducing ammonia levels is crucial, as the wastewater is often discharged directly into surrounding rivers without prior treatment. Table 5 presents the ammonia concentrations before and after the adsorption process in shrimp pond wastewater.

Table 5. Ammonia content before and after adsorption in shrimp pond wastewater.

Locations	Initial ammonia concentration (mg/L)	Final ammonia concentration (mg/L)	% Adsorption	Adsorption capacity (mg/g)
1A	15.4	7.1	53.8	8.3
1B	16.9	6.2	63.4	10.8
1C	11.9	5.7	52.2	6.2
1D	13.9	6.7	52.1	7.3
2A	35.6	4.7	86.8	30.9
2B	32.6	8.4	74.4	24.3
2C	35.2	7.6	78.5	27.6
2D	38.8	11.5	70.5	27.3
3A	30.9	9.4	69.6	21.6
3B	25.5	7.4	71.1	18.2
3C	34.8	8.1	76.7	26.7
3D	31.3	13.9	55.6	17.4
4A	29.8	10.3	65.4	19.5
4B	28.4	12.5	56.1	16.0
4C	27.9	12.1	56.7	15.9
4D	31.6	10.9	65.4	20.6

After the adsorption process using $Fe_3O_4/SiO_2/CaCO$ adsorbents, the ammonia content in the shrimp ponds decreased significantly. The reduction in ammonia concentration achieved adsorption efficiencies ranging from 52.1% to 86.8%, with adsorption capacities between 6.2 and 30.9 mg/g.

The FT-IR spectra of $Fe_3O_4/SiO_2/CaCO_3$ adsorbent, before and after ammonia adsorption, are compared in Figure 11. The figure reveals a shift in the absorption band from 798.53 to 713.66 cm^{-1}, corresponding to the Si-O stretching vibration of Si-O-Si. Additionally, the absorption at 1478.35 cm^{-1}, attributed to the stretching vibration of the C-O-H bond before adsorption, shifts to 1447.76 cm^{-1} as a bending vibration after adsorption. This decrease in wavenumber indicates interaction between the group and ammonia during the adsorption process. There is also a shift in the wavenumber from 2509.39 cm^{-1} before adsorption to 2511.32 cm^{-1} after adsorption, representing the stretching vibration of the O-H bond (carboxylic acid). Furthermore, the shift from 3244.27 cm^{-1} to 3307.92 cm^{-1} reflects the stretching vibration of the OH group in the silanol group, indicating interaction with ammonia.

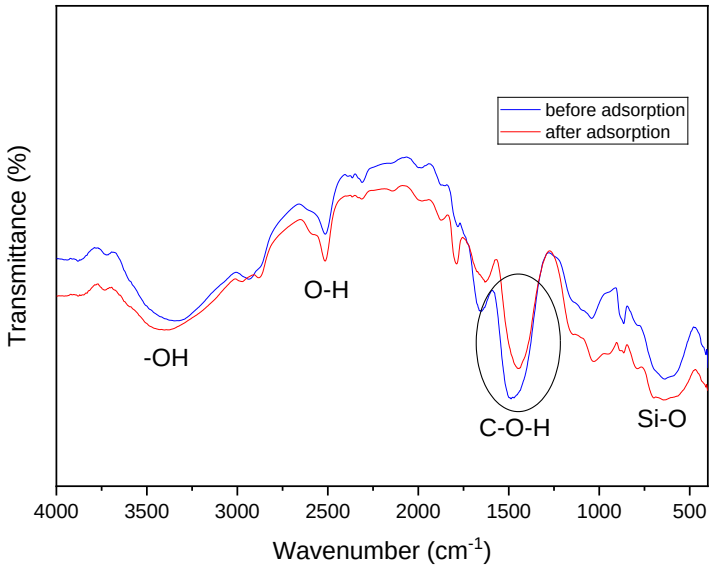

Figure 11. FT-IR spectra of $Fe_3O_4/SiO_2/CaCO_3$ adsorbent before and after adsorption.

4. Conclusions

The synthesis of $CaCO_3$ from coral skeleton, SiO_2 from sand, and $Fe_3O_4/SiO_2/CaCO_3$ adsorbent was successfully achieved, as confirmed by XRF, FTIR, and XRD characterizations. The adsorption process adhered to the second-order kinetics model, exhibited spontaneous behavior with a negative ΔG value, and followed the Langmuir isotherm model ($R^2 = 0.9267$). Optimal conditions for ammonia adsorption by the $Fe_3O_4/SiO_2/CaCO_3$ adsorbent in a 25 mL standard solution of 4 mg/L ammonia standard solution were determined to be a mass of 0.025 g, a contact time of 60 minutes, a temperature of 27 °C, and a pH of 5, achieving an adsorption efficiency of 89.3%. When applied to shrimp pond wastewater, the $Fe_3O_4/SiO_2/CaCO_3$ adsorbent demonstrated an adsorption efficiency ranging from 52.1% to 86.8% and an adsorption capacity between 6.2 and 30.9 mg/g.

Use of AI tools declaration

The authors declare they have not used Artificial Intelligence (AI) tools in the creation of this article.

Acknowledgments

This research was supported by the PNBP Universitas Negeri Malang through Thesis Research Grant 2023, No. 5.4.1/UN32/KP/2023. We express their gratitude to the editor and reviewers for their comments to improve the manuscript significantly.

Conflict of interest

The authors stated that there is no conflict of interest for the study.

References

1. Wijaya AR, Arifani RI, Kusumaningrum IK, et al. (2019) *Analysis of Fe in sediment material using a modified Tessier technique for detection of Fe-anthropogenic and Fe-naturals*, IOP Conference Series: Materials Science and Engineering, IOP Publishing, 515: 012015. https://doi.org/10.1088/1757-899X/515/1/012015
2. Wijaya AR, Khoerunnisa F, Armid A, et al. (2022) The best-modified BCR and Tessier with microwave-assisted methods for leaching of Cu/Zn and their δ65Cu/δ66Zn for tracing sources in marine sediment fraction. *Environ Technol Inno* 28: 102663. https://doi.org/10.1016/j.eti.2022.102663
3. Suci CW, Wijaya AR, Santoso A, et al. (2020) *Fe leaching in the sludge sediment of the prigi beach with Tessier-microwave method*, AIP Conference Proceedings, AIP Publishing, 2231. https://doi.org/10.1063/5.0002589
4. Wijaya AR, Oktaviana I, Wonorahardjo S, et al. (2019) *Optimization of BCR microwave from Fe assessment in sediment material in the Gulf of Prigi*, IOP Conference Series: Materials Science and Engineering, IOP Publishing, 515: 012091. https://doi.org/10.1088/1757-899X/515/1/012091
5. Wang Z, Xu J, Hu Y, et al. (2016) Functional nanomaterials: Study on aqueous Hg(II) adsorption by magnetic Fe_3O_4@SiO_2-SH nanoparticles. *J Taiwan Inst Chem E* 60: 394–402. https://doi.org/10.1016/j.jtice.2015.10.041
6. Crini G, Lichtfouse E, Wilson LD, et al. (2019) Conventional and non-conventional adsorbents for wastewater treatment. *Environ Chem Lett* 17: 195–213. https://doi.org/10.1007/s10311-018-0786-8
7. Sasongko A (2018) Ammonia determination in bottled water using spectrophotometer: Comparison between Nessler and Berthelot methods. *JST* 7: 126–134. https://doi.org/10.23887/jst-undiksha.v7i1.13009
8. Tran TN, Pham TVA, Le MLP, et al. (2013) Synthesis of amorphous silica and sulfonic acid functionalized silica used as reinforced phase for polymer electrolyte membrane. *Adv Nat Sci Nanosci* 4. https://doi.org/10.1088/2043-6262/4/4/045007
9. Jiang Y, Jiang FQ, Liao X, et al. (2020) Customized three-dimensional porous catalyst for Knoevenagel reaction. *J Porous Mat* 27: 779–788. https://doi.org/10.1007/s10934-020-00859-3
10. C. Matei, D. Berger, A. Dumbrava, et al. (2020) Calcium carbonate as silver carrier in composite materials obtained in green seaweed extract with topical applications. *J Sol-Gel Sci Techn* 93: 315–323. https://doi.org/10.1007/s10971-019-05145-6
11. Nanlohy F, Wijaya AR, Semedi B (2021) Synthesis of Fe_3O_4/MnO_2/Humic acid nanocomposite for strontium ion adsorption and its interferences, In AIP Conference Proceedings, 2353: 030108. https://doi.org/10.1063/5.0052981
12. Wonorahardjo S, Fajaroh F, Joharmawan R, et al. (2023) Cadmium and lead ions adsorption on magnetite, silica, alumina, and cellulosic materials. *Sci Rep* 13: 1–15. https://doi.org/10.1038/s41598-023-30893-5
13. Jin Q, Huang L, Li A, et al. (2017) Quantification of the limitation of Langmuir model used in adsorption research on sediments via site energy heterogeneity. *Chemosphere* 185: 518–528. https://doi.org/10.1016/j.chemosphere.2017.07.051

14. Al-Ghouti MA, Da'ana DA (2020) Guidelines for the use and interpretation of adsorption isotherm models: A review. *J Hazard Mater* 393: 122383. https://doi.org/10.1016/J.JHAZMAT.2020.122383